

pubs.acs.org/NanoLett Letter

Atomic-Resolution Imaging of Small Organic Molecules on Graphene

Priti Kharel, Blanka E. Janicek, Sang hyun Bae, Amanda L. Loutris, Patrick T. Carmichael, and Pinshane Y. Huang*



Cite This: https://doi.org/10.1021/acs.nanolett.2c00213



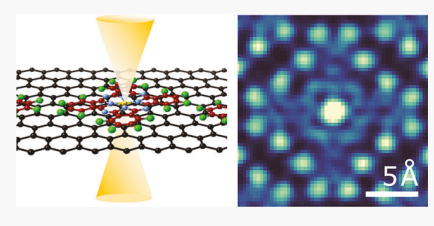
ACCESS

III Metrics & More



sı Supporting Information

ABSTRACT: Here, we demonstrate atomic-resolution scanning transmission electron microscopy (STEM) imaging of light elements in small organic molecules on graphene. We use low-dose, room-temperature, aberration-corrected STEM to image 2D monolayer and bilayer molecular crystals, followed by advanced image processing methods to create high-quality composite images from $\sim 10^2 - 10^4$ individual molecules. In metalated porphyrin and phthalocyanine derivatives, these images contain an elementally sensitive contrast with up to 1.3 Å resolution—sufficient to distinguish individual carbon and nitrogen atoms. Importantly, our methods can be applied to



molecules with low masses (\sim 0.6 kDa) and nanocrystalline domains containing just a few hundred molecules, making it possible to study systems for which large crystals cannot easily be grown. Our approach is enabled by low-background graphene substrates, which we show increase the molecules' critical dose by 2–7×. These results indicate a new route for low-dose, atomic-resolution electron microscopy imaging to solve the structures of small organic molecules.

KEYWORDS: structure determination, small organic molecules, scanning transmission electron microscopy, atomic resolution, graphene support

benchmark in small-molecule structure characterization This the ability to image the arrangements of carbon and other light elements in a monolayer or submonolayer of molecules. In this limit, the structure of a molecule can be directly "read" off of one or more real-space images, sidestepping the potential for structural misassignments that can occur with less direct methods. Indeed, atom connectivities in individual small molecules have been imaged using noncontact atomic force microscopy and scanning tunneling microscopy, but these techniques cannot easily elucidate nonplanar structures or provide a direct elemental identification of atoms. 1,2 On the other hand, single-particle cryoelectron microscopy (cryo-EM) has become a gold standard for the high-resolution structure determination of biological macromolecules³ but is limited to large molecules of ~40 kDa or more^{4,5} because of their higher image contrast. Obtaining similar capabilities for small organic molecules has enormous potential. A real-space route to small-molecule structures can be highly complementary to diffraction methods such as X-ray crystallography⁶ and microcrystal electron diffraction (microED)^{7,8} because it does not require input models and avoids the challenges associated with inverting real-space structures from diffraction data. Indeed, thick crystals of small molecules have been imaged in (S)TEM since the 1970s, 9-16 in part to acquire more accurate phase information for electron crystallography. Meanwhile, real-space imaging is intrinsically well suited to analyzing extremely small volumes of materials, including nanocrystalline or even amorphous samples—as well

as understanding the arrangement of molecules on surfaces, including the structure of organic/inorganic 2D heterostructures. ¹⁷ Driven by such merits, imaging methods have advanced considerably for 2D¹⁸ or 3D polymers ¹⁹ and MOFs, ^{20–24} but new approaches are needed for small molecules, which require tailored strategies for sample preparation and analysis.

The key challenge for imaging small organic molecules with electron microscopy is that small molecules combine weak electron scattering with high sensitivity to radiation damage, $^{25-27}$ making it difficult to extract a molecule's atomic structure without modifying it. For example, while several studies have shown that single molecules can be imaged using graphene or carbon nanotube substrates when high electron doses are applied $(\sim \! 10^4 - \! 10^6 \ e^-/\mbox{Å}^2),^{28-31}$ the rapid structural transformations induced by this approach makes it better suited toward investigating atomic rearrangements and chemical reactions than for a structural determination of unknown analytes. An alternate approach is to acquire low-dose images and then combine signals from many individual molecules to recover a high-quality image. When it is applied

Received: January 17, 2022 Revised: April 7, 2022



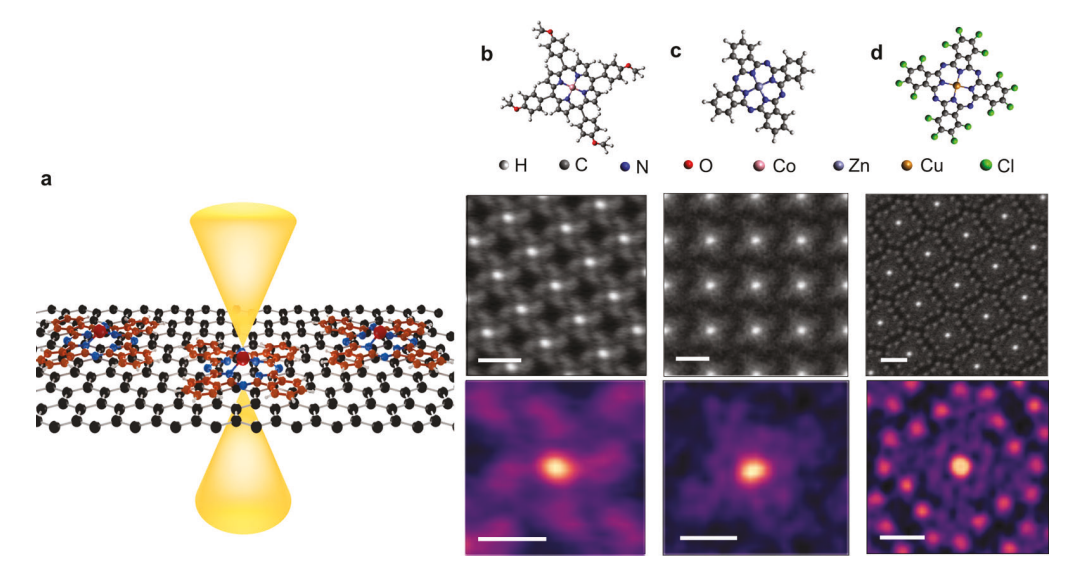


Figure 1. Atomic-scale and atomic-resolution imaging of organic molecules using ADF-STEM. (a) Schematic of the experiment: one to two layers of molecules are evaporated onto suspended graphene and imaged using aberration-corrected ADF-STEM. (b-d) 2D structural representations (top) and experimental averaged images (middle and bottom) of (b) CoTMPP, (c) ZnPc, and (d) CuPcCl. The middle row of images shows the arrangement of molecules in each 2D crystal, and the bottom row shows a magnified, low-pass filtered image of one molecule. Data for CoTMPP were acquired from a bilayer, while ZnPc and CuPcCl data were from a monolayer of molecules. Image processing methods are detailed in the Supporting Information. Scale bars are 1 nm (middle) and 5 Å (bottom).

to small molecules, this method has so far only been successful for recovering relatively large signals—either for imaging thick crystals $^{10-13,15}$ or for detecting heavy elements. For example, at the monolayer limit, signal averaging has been used to locate copper and chlorine in chlorinated copper phthalocyanine, 32 but not the light elements that are key to understanding the structure of organic molecules. Driven by the intense interest in single-particle analysis in the cryo-EM community, data processing techniques for extracting molecular structure from large, noisy data sets have advanced rapidly. 33,34 Recently, data methods borrowed or adapted from cryo-EM have begun to spill over to other fields. These advances point to new opportunities to apply atomic-resolution, low-dose imaging to determine the structures of small organic molecules directly from atomically thin samples. Here, we adapt data processing techniques from 2D electron crystallography 36,37 and singleparticle analysis to recover atomic-scale information acquired from monolayer and bilayer small-molecule crystals on graphene. Using these methods, we obtain 2D elementally sensitive images of planar molecules with up to atomic resolution (1.3 Å), rivaling the 3D resolution of state of the art cryo-EM, 38,39 but for molecules 2 orders of magnitude lower in mass.

Figure 1 shows averaged annular dark-field (ADF) STEM images acquired at room temperature from 2D crystals of three metal complexes: cobalt(II) *meso*-tetrakis(4-methoxyphenyl)-porphyrin (CoTMPP; Figure 1b), zinc phthalocyanine (ZnPc, Figure 1c), and chlorinated copper phthalocyanine (CuPcCl, Figure 1d). Porphyrins and phthalocyanines represent two broadly important classes of molecules that include natural products, such as heme and chlorophyll, as well as molecules used for catalysis, dyes, and organic electronics. 40-42 These molecules are also ideal test systems for high-resolution imaging. First, they are quasi-planar and are arranged flat on the graphene substrate, 43 making it possible to determine their structure from 2D images acquired at a single orientation. Second, while highly conjugated aromatic molecules are

relatively robust to radiation damage, ²⁷ these three molecules also represent a range of beam sensitivities spanning 2 orders of magnitude, from $\sim 10^1$ to 10^3 e⁻/Å² (see Table S2). Finally, the molecules contain metal atoms which facilitate automated molecular detection (see the Supporting Information). To prepare these samples for imaging, we thermally evaporated each molecule onto homemade suspended graphene TEM grids, ⁴⁴ producing nanocrystals ranging from 50 to hundreds of nanometers across (see Figure 3a-c) and 1–2 molecules thick, as measured using quantitative ADF-STEM (see the Supporting Information).

As illustrated by Figure 1a, we imaged the molecular crystals using low-angle ADF-STEM at 300 kV (see the Supporting Information for acquisition details). In STEM, an angstromscale electron beam (approximately 0.8 Å for our experimental setup) is scanned along the sample, and scattered electrons are collected as a function of the probe position. ADF-STEM produces elementally sensitive Z-contrast images in which the contrast for an individual atom scales with the atomic number Z^{γ} , where γ ranges from 1.2 to 2 depending on the inner collection angle of the ADF detector. 25,45 Our simulations show that, at the single-atom limits, low-angle ADF-STEM offers a signal to noise ratio for light element imaging comparable to or better than that for annular bright-field STEM with the additional advantage of being directly interpretable (see Figure S2). These data are consistent with previous simulation results,²⁵ which indicated that low-angle ADF-STEM is an ideal method for imaging single molecules despite a commonly held belief that ADF-STEM is less dose efficient than bright-field STEM or TEM. When it is applied to 2D crystals of small organic molecules, ADF-STEM thus offers, in principle, the ability to solve molecular structures directly from one or more 2D images.

As shown in Figure 1b-d, our methods produce high-resolution, averaged images of 2D aromatic molecules that reveal remarkable detail. For example, images of bilayer CoTMPP reveal the orientation of methoxyphenyl groups,

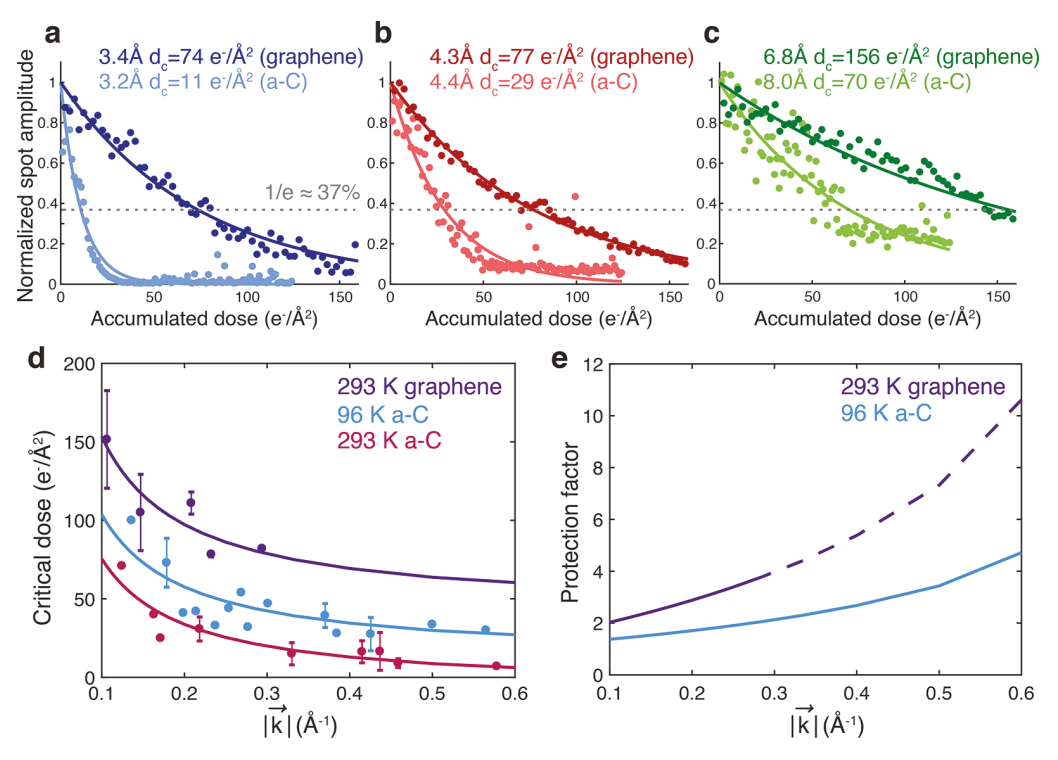


Figure 2. Effect of graphene substrates on the critical dose (d_c) of CoTMPP. (a—c) Normalized electron diffraction spot amplitude as a function of the accumulated electron dose of bulk crystals on a-C and bilayer crystals on graphene. The data (points) and exponential fit (line) are plotted for both the a-C (light color) and graphene (dark color) crystals, with the 1/e d_c cutoff is indicated by a gray dashed line. Because the crystal structures and zone axes differ between the two samples, we compare the most similar d spacings. We obtain d_c values of 11-70 e⁻/Ų for bulk crystals on a-C and 74-156 e⁻/Ų for thin crystals on graphene. (d) Critical dose as a function of scattering vector. We compared d_c measured for 2D crystals on graphene substrates at room temperature (purple), bulk crystals on a-C at room temperature (red), and bulk crystals on a-C at 96 K (blue). Each point represents the average d_c value measured from multiple crystals for each k vector, and the error bars represent the standard deviation. (e) The protection factor versus scattering vector k, obtained by taking a ratio of best-fit curves from the data in (d). Solid lines indicate data obtained from the measured range of k vectors, while dashed lines are an extrapolation. For all k vectors measured, graphene offers a greater protection than cryogenic cooling.

which appear as propeller-like features around the bright cobalt center (Figure 1b). For monolayer ZnPc (Figure 1c), we can locate the metal center, visualize the 4-fold symmetry of the molecule, and even distinguish the carbon rings in the macrocycle, such as the benzene rings at the edge of the molecule. Our images of monolayer CuPcCl reveal the light elements in the connecting macrocycle as well as the structure of the four isoindole rings between the metal atom at the center and the chlorine atoms at the edge (Figure 1d). Each of these images represents data collected from between 100 and 12000 individual molecules, comparable to those typically used for each projection in cryo-EM. 38,39,46 Importantly, these molecules can be obtained from extremely small regions; for instance, Figure 1b is generated from 2000 molecules, each located in a single crystal domain only 50 nm across. By fitting the apparent size of the metal atoms and comparing the averaged images to simulations, we find that the effective resolution of the class averages is 2.0 Å for CoTMPP and 1.9 Å for ZnPc (see the Supporting Information). As we discuss later, we obtain the highest effective spatial resolution of 1.3 Å in CuPcCl.

To obtain these images, a key first step is to detect individual small molecules in electron microscopy images while minimizing structural changes induced by electron beam damage. Unlike 2D polymers and MOFs, which are relatively mechanically robust and can often be grown in large, self-supporting crystals, 18,22,24 monolayer small molecules require a

TEM support substrate. For our imaging studies, we utilize graphene substrates, a one-atom-thick layer of carbon atoms, which is the lowest-possible background support membrane for (S)TEM. 32,47-51 Graphene is also thought to increase a material's resistance to electron irradiation because of its high electrical conductivity, high thermal conductivity, and impermeability, 52,53 though this effect has never been directly quantified for small molecules. To evaluate the potential of graphene grids for enabling atomic-scale small molecule imaging, we studied the effect of graphene substrates on the radiation sensitivity of CoTMPP. We fabricated two types of CoTMPP samples: conventional samples prepared through dry deposition of bulk crystals, measured by atomic force microscopy to be 40-200 nm thick, on amorphous carbon (a-C) grids and bilayer crystals evaporated onto graphene grids. We then measured the critical dose, a measure of the beam sensitivity of a material, using selected area electron diffraction at 300 kV (see the Supporting Information). Figure 2a-d compares the critical doses of bulk crystals on conventional grids to 2D crystals on graphene. We find that graphene increases the dose resistance of CoTMPP at all scattering vectors. For example, in Figure 2a, we obtained a room-temperature $d_c = 11 \text{ e}^{-}/\text{Å}^2$ for the 3.2 Å diffraction spot of bulk CoTMPP on a-C but $d_c = 74 \text{ e}^{-}/\text{Å}^2$ for the 3.4 Å diffraction spot of bilayer CoTMPP on graphene.

By taking the ratio of the critical doses of the 2D sample on graphene with respect to the bulk sample, we calculate the

protection factor that graphene provides to the molecules. Figure 2e plots the protection factor versus scattering vector k. We obtain protection factors of between 2 and 7 for the k vectors we measured, comparable to the 9× protection factor graphene provides to inorganic materials. The highest protection factors are observed for larger scattering vectors, indicating that graphene is most effective at preserving the high-frequency information needed for atomic-scale imaging. Notably, Figure 2e shows that, for the highest k vector measured, graphene's protection factor is approximately more than 2 times larger than that obtained by cryogenic cooling of bulk samples to 96 K. Together, these results show that graphene substrates can play a significant role in enabling atomic-scale imaging of small molecules.

In addition to graphene substrates, a second key step to minimize changes to the molecular structure is to limit their electron exposure. We use a low-dose, low-magnification imaging procedure, as detailed in the Supporting Information, to locate the 2D molecular crystals of interest. Figure 3a–c shows the resulting images: for example, Figure 3a shows the highly faceted crystals of bilayer CoTMPP, highlighted in gold in the bottom half of the image. Next (Figure 3d–f), we acquire low-dose, high-magnification images within a single crystal. We tailored the electron dose to the beam sensitivity of each molecule on graphene, ranging from 50 to 660 e $^-/\mbox{Å}^2$ for

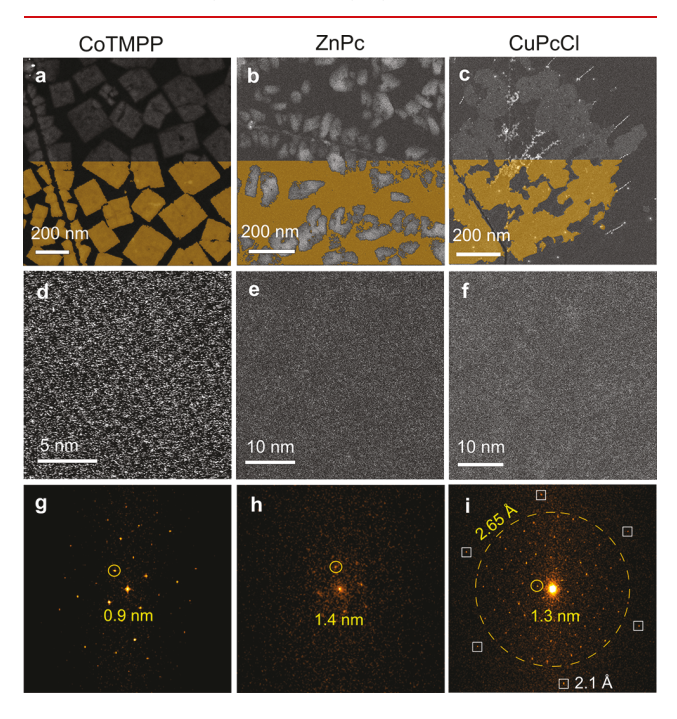


Figure 3. ADF-STEM image acquisition procedure for 2D molecular crystals. (a–c) Low-magnification images showing the morphology of as-deposited crystals on graphene. Gold indicates regions with thin crystals of (a) bilayer CoTMPP, (b) monolayer ZnPc, and (c) monolayer CuPcCl. While the bilayer CoTMPP crystals are highly faceted, ZnPc and CuPcCl form sheets, sometimes dotted with small crystals of thicker material (white regions in (b)). (d–f) Low-dose images acquired using 48, 118, and 661 e $^-/{\rm A}^2$. Faint lattice fringes are visible in each image, but the molecular structure is obscured by noise. (g–i) Fast Fourier transforms (FFT) of the regions in (d–f) show periodic peaks from the molecular crystals and demonstrate information transfer up to 2.65 Å for CuPcCl (i). The innermost reflections are marked for each molecular crystal for scale. The 6-fold graphene reflections at 2.1 Å are also visible, marked by squares in (i).

the molecules we studied (see the Supporting Information and Table S1). In these low-dose images, the crystal lattice is visible as a series of weak fringes, but the structure of individual molecules is obscured by noise. Despite the low signal to noise, the fast Fourier transforms (FFTs) (Figure 3g–i) show that these images contain atomic-scale information; peaks in the FFT are visible up to 2.65 Å for CuPcCl and 2.1 Å for graphene. These values do not represent a limit on the information present in the image and can improve beyond 2 times the initial limit with averaging because real- or Fourier-space alignment methods effectively sharpen peaks in the FFT so that they become visible above the noise background. S4–S6 Once we acquire low-dose images of each molecular crystal, we extract the atomic-scale structure using the class averaging approach illustrated in Figure 4 for CoTMPP. First, we applied

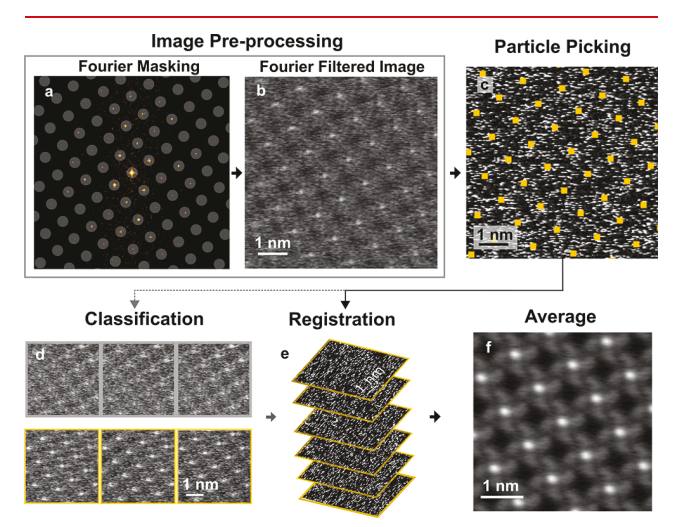


Figure 4. Schematic of our class averaging process. (a) We apply a mask to the fast Fourier transform of the image, producing (b) a Fourier-filtered image where the (c) metal centers of the molecules are readily identified. Next, we optionally refine the particles using image classification to remove "bad" classes of particles. (d) Images from two representative classes. The images in the bottom class (yellow) have higher contrast than images in the "bad" class (gray). (e) Images from the "good" class (2000 frames) are registered and averaged to generate (f) the final average.

a Fourier filter (Figure 4a,b) to isolate the periodic signal from the 2D lattice (see the Supporting Information), a technique commonly used in electron crystallography to reduce background noise. ^{56,57} We then segment each image into small regions centered around each molecule (Figure 4c). An optional next step is image classification and refinement (Figure 4d). The segmented images are registered (Figure 4e) and averaged to obtain the final image (Figure 4f).

As we show below, advanced data averaging methods are key to producing directly interpretable, atomic-resolution images of small molecules from low-dose STEM images. We explored three averaging approaches with increasing levels of sophistication: (1) threshold-based averaging, (2) reference-based averaging, and (3) iterative classification. We applied each method to an image of monolayer CuPcCl. To compare improvements in image quality among the different image averaging methods, we consider the effective resolution of the final averaged image. We note that this resolution is distinct from the intrinsic microscope resolution (\sim 0.8 Å for our experimental setup) in that it contains contributions from the

probe size as well as blurring from imperfect image registration and averaging of nonidentical objects, similar to the resolution of the 3D reconstruction in single-particle analysis. ⁵⁶ For data processing details and comparisons of these methods, see the Supporting Information and Table S3.

Figure 5a,b shows that threshold- and reference-based averaging—methods that simply locate, align, and average

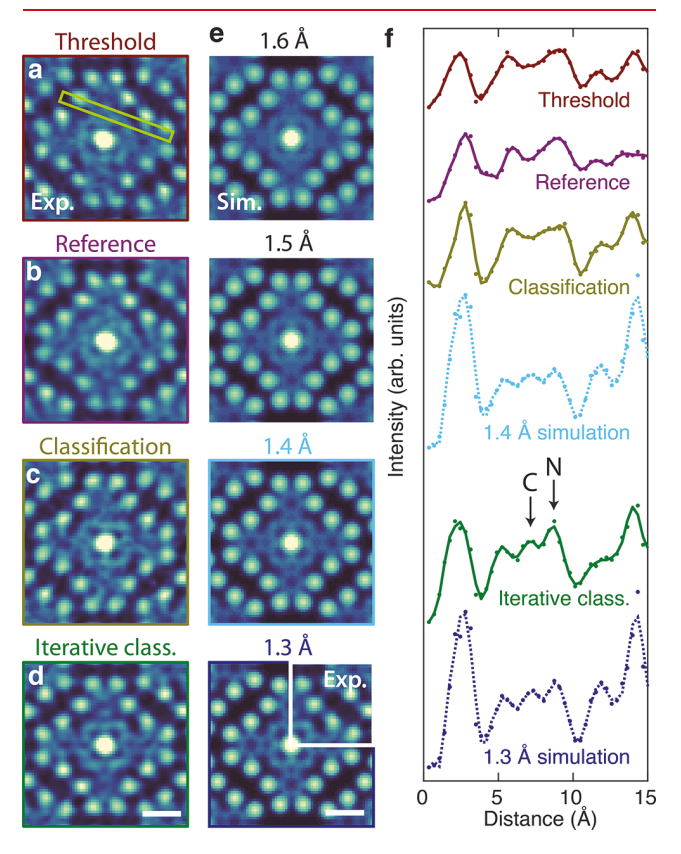


Figure 5. Data processing methods for atomic resolution imaging of monolayer CuPcCl. (a-d) Experimental ADF-STEM data after processing using (a) threshold-based averaging (1372 frames), (b) reference-based averaging (3924 frames), (c) a single round of classification (320 frames), and (d) iterative classification (140 frames). All images are low-pass filtered. (e) Multislice ADF-STEM simulations of monolayer CuPcCl with probe sizes (fwhm) from 1.3 to 1.6 Å. The upper right corner of the 1.3 Å simulation is overlaid with a quadrant of the experimental image in (d). (f) Line profiles across a C-N bond, indicated by the green rectangle in (a). Data are shown as points, displayed with a smoothed (Savitsky-Golay filtered) line as a guide to the eye. In the iterative class average, intensity peaks corresponding to individual C and N atoms are visible, and N atoms appear brighter than C atoms. We estimate that the resolution obtained using the iterative classification method is 1.3 Å. Scale bars are 5 Å.

individual frames and have been previously used to increase the signal-to-noise ratio SNR of molecules on graphene 32 —produce comparable averages. Here, we see that these methods are sufficient to reveal the positions of the heavier Cu and Cl atoms as well as weaker contrast from the inner macrocycle of the phthalocyanine. In comparison to multislice image simulations 58 with varying probe sizes (Figure 5e), the experimental data in Figure 5a,b are consistent with an effective probe fwhm of ~ 1.6 Å (see the Supporting Information for image simulation details). While probe size is often used as a proxy for resolution in inorganic specimens,

Fourier ring correlation (FRC) is a commonly used metric to quantify resolution in 2D projections of cryo-EM data. 59 Using FRC on Figure 5a, we measured 1.0 Å resolution (see Figure S6). Both of these metrics indicate that the averaged images contain angstrom-scale information. Despite the high measured spatial resolution of our averages, clear distortions are present in the experimental averages: for example, the four inner pyrrole rings are asymmetric across the metal center and their ring structure is poorly defined, making it difficult to extract the position of light atoms from the averaged image. These distortions likely result from errors in the alignment between frames or the inclusion of misidentified or damaged molecules. Images in Figure 5c,d are generated from the same raw data but are processed using either a single (Figure 5c) or multiple iterative classification cycles (Figure 5d) implemented via EMAN2, an open-source image processing software for single-particle analysis.⁶⁰ In each cycle, particles are classified using the software's built-in principal component analysis and k-means classification tools. Particles in the class(es) that produce the highest resolution averaged image are retained (see the Supporting Information). We believe this process removes relatively damaged, poorly centered, and misidentified regions from the final class average.

We obtain the best average image (Figure 5d) from multiple cycles of iterative classification. Here, the porphyrazine ring around the metal center as well as the five- and six-membered rings of the isoindole groups are clearly visible. By taking line profiles of the image intensity across the azomethine C–N bond for each averaging method and comparing them to simulated data (Figure 5f), we demonstrate that we can resolve individual carbon and nitrogen atoms in the iterative class average and achieve an effective resolution of \sim 1.3 Å. In Figure 5f (green), we measure a C–N bond length of 1.4 \pm 0.1 Å, consistent with the 1.35 Å bond length reported for bulk crystals of β -copper phthalocyanine. In the 2D image and line profile, we are also able to distinguish nitrogen and carbon atoms on the basis of their intensities, which is higher for nitrogen because of its larger atomic number.

Together, this work demonstrates a new method to image and understand the structures of small molecules, atom by atom, with up to 1.3 Å resolution in nanoscale molecular crystals. Our methods produce direct, real-space, elementally sensitive images of the molecular structure and require crystals just a few hundred molecules across, representing a potentially powerful new tool for ab initio small-molecule structure determination. While our work demonstrates new methods to create high-resolution 2D projection images of planar or quasi-planar molecules, our approach may be extended to determine the full 3D structure of molecules by capturing images from multiple projections to produce 3D reconstructions. In addition, because our techniques can access both the structure and arrangements of molecules on surfaces, we believe our methods should be useful for studying soft-hard interfaces such as mixed organic/inorganic van der Waals heterostructures. Finally, our data analysis approach and insights into the protection factor of graphene can advance imaging of beam-sensitive materials, such as 2D polymers and MOFs. Overall, this study represents a powerful new pathway to visualize and understand beam-sensitive organic systems at the atomic and molecular limits using electron microscopy.

ASSOCIATED CONTENT

Supporting Information

The Supporting Information is available free of charge at https://pubs.acs.org/doi/10.1021/acs.nanolett.2c00213.

TEM sample fabrication, STEM acquisition, molecular thickness determination, critical dose measurements, and averaging procedure and analysis (PDF)

AUTHOR INFORMATION

Corresponding Author

Pinshane Y. Huang — Department of Materials Science and Engineering, University of Illinois Urbana—Champaign, Urbana, Illinois 61801, United States; Materials Research Laboratory, University of Illinois at Urbana—Champaign, Urbana, Illinois 61801, United States; orcid.org/0000-0002-1095-1833; Email: pyhuang@illinois.edu

Authors

Priti Kharel — Department of Chemistry, University of Illinois Urbana—Champaign, Urbana, Illinois 61801, United States; orcid.org/0000-0002-1933-8242

Blanka E. Janicek – Department of Materials Science and Engineering, University of Illinois Urbana–Champaign, Urbana, Illinois 61801, United States; o orcid.org/0000-0002-5529-2819

Sang hyun Bae – Department of Materials Science and Engineering, University of Illinois Urbana–Champaign, Urbana, Illinois 61801, United States

Amanda L. Loutris — Department of Materials Science and Engineering, University of Illinois Urbana—Champaign, Urbana, Illinois 61801, United States

Patrick T. Carmichael – Department of Materials Science and Engineering, University of Illinois Urbana–Champaign, Urbana, Illinois 61801, United States

Complete contact information is available at: https://pubs.acs.org/10.1021/acs.nanolett.2c00213

Author Contributions

 $^{\parallel}$ P.K. and B.E.J. contributed equally to this work.

The authors declare no competing financial interest.

■ ACKNOWLEDGMENTS

This work was carried out in part in Materials Research Laboratory Central Facilities at the University of Illinois, where electron microscopy and deposition facilities were supported by J. Mabon, C. Q. Chen, and A. Sibert. The authors thank J. Vura-Weiss, K. Zhang, and A. Sharma for the use of their thermal evaporator and J. Rodríguez-López and N. B. Schorr for providing chemicals. The authors acknowledge useful discussions with B. K. Clark, A. Khan, A. Schleife, B. Robinson, C. J. Murphy, J.-M. Zuo, and C.-H. Lee. This work was supported primarily by a Packard foundation fellowship. Additional support from an NSF CAREER award DMR-1846206 was used to develop the graphene substrates. This work utilized facilities provided by the NSF-MRSEC award number DMR-1720633.

■ REFERENCES

(1) Gross, L.; Schuler, B.; Pavliček, N.; Fatayer, S.; Majzik, Z.; Moll, N.; Peña, D.; Meyer, G. Atomic Force Microscopy for Molecular Structure Elucidation. *Angew. Chem., Int. Ed.* **2018**, *57*, 3888–3908.

- (2) Temirov, R.; Soubatch, S.; Neucheva, O.; Lassise, A. C.; Tautz, F. S. A novel method achieving ultra-high geometrical resolution in scanning tunnelling microscopy. *New J. Phys.* **2008**, *10*, 053012.
- (3) Henderson, R. From Electron Crystallography to Single Particle CryoEM (Nobel Lecture). *Angew. Chem., Int. Ed.* **2018**, *57*, 10804–10825.
- (4) Glaeser, R. M. How good can cryo-EM become? *Nat. Methods* 2016, 13, 28-32.
- (5) Fan, X.; Wang, J.; Zhang, X.; Yang, Z.; Zhang, J.-C.; Zhao, L.; Peng, H.-L.; Lei, J.; Wang, H.-W. Single particle cryo-EM reconstruction of 52 kDa streptavidin at 3.2 Angstrom resolution. *Nat. Commun.* **2019**, *10*, 2386.
- (6) Dunitz, J. D. X-ray analysis and the structure of organic molecules, 2nd ed.; Verlag Helvetica Chimica Acta: 1995.
- (7) Jones, C. G.; Asay, M.; Kim, L. J.; Kleinsasser, J. F.; Saha, A.; Fulton, T. J.; Berkley, K. R.; Cascio, D.; Malyutin, A. G.; Conley, M. P.; Stoltz, B. M.; Lavallo, V.; Rodríguez, J. A.; Nelson, H. M. Characterization of Reactive Organometallic Species via MicroED. ACS Central Science 2019, 5, 1507–1513.
- (8) Gruene, T.; et al. Rapid Structure Determination of Microcrystalline Molecular Compounds Using Electron Diffraction. *Angew. Chem., Int. Ed.* **2018**, *57*, 16313–16317.
- (9) Uyeda, N.; Kobayashi, T.; Suito, E.; Harada, Y.; Watanabe, M. Molecular image resolution in electron microscopy. *J. Appl. Phys.* **1972**, *43*, 5181–5189.
- (10) Uyeda, N.; Kobayashi, T.; Ishizuka, K.; Fujiyoshi, Y. High Voltage Electron Microscopy for Image Discrimination of Constituent Atoms in Crystals and Molecules. *Chemica scripta* **1979**, *14*, 47–61.
- (11) Kobayashi, T.; Fujiyoshi, Y.; Iwatsu, F.; Uyeda, N. Highresolution TEM images of zinc phthalocyanine polymorphs in thin films. *Acta Crystallogr., Sect. A* 1981, 37, 692–697.
- (12) Kirkland, E. J.; Siegel, B. M.; Uyeda, N.; Fujiyoshi, Y. Improved high resolution image processing of bright field electron micrographs: II. Experiment. *Ultramicroscopy* **1985**, *17*, 87–103.
- (13) Kobayashi, T.; Ogawa, T.; Moriguchi, S.; Suga, T.; Yoshida, K.; Kurata, H.; Isoda, S. Inhomogeneous substitution of polyhalogenated copper-phthalocyanine studied by high-resolution imaging and electron crystallography. *Journal of Electron Microscopy* **2003**, *52*, 85–90
- (14) Haruta, M.; Yoshida, K.; Kurata, H.; Isoda, S. Atomic resolution ADF-STEM imaging of organic molecular crystal of halogenated copper phthalocyanine. *Ultramicroscopy* **2008**, *108*, 545–551.
- (15) Haruta, M.; Kurata, H. Direct observation of crystal defects in an organic molecular crystals of copper hexachlorophthalocyanine by STEM-EELS. *Sci. Rep.* **2012**, *2*, 2–5.
- (16) Yoshida, K.; Biskupek, J.; Kurata, H.; Kaiser, U. Critical conditions for atomic resolution imaging of molecular crystals by aberration-corrected HRTEM. *Ultramicroscopy* **2015**, *159*, 73–80.
- (17) Xu, X.; Lou, Z.; Cheng, S.; Chow, P. C.; Koch, N.; Cheng, H. M. Van der Waals organic/inorganic heterostructures in the two-dimensional limit. *Chem.* **2021**, *7*, 2989–3026.
- (18) Qi, H.; et al. Near-atomic-scale observation of grain boundaries in a layer-stacked two-dimensional polymer. *Science Advances* **2020**, *6*, No. eabb5976.
- (19) Jiang, X.; Greer, D. R.; Kundu, J.; Ophus, C.; Minor, A. M.; Prendergast, D.; Zuckermann, R. N.; Balsara, N. P.; Downing, K. H. Imaging Unstained Synthetic Polymer Crystals and Defects on Atomic Length Scales Using Cryogenic Electron Microscopy. *Macromolecules* **2018**, *51*, 7794–7799.
- (20) Zhu, Y.; Ciston, J.; Zheng, B.; Miao, X.; Czarnik, C.; Pan, Y.; Sougrat, R.; Lai, Z.; Hsiung, C.-E.; Yao, K.; Pinnau, I.; Pan, M.; Han, Y. Unravelling surface and interfacial structures of a metal—organic framework by transmission electron microscopy. *Nat. Mater.* **2017**, *16*, 532–536.
- (21) Zhang, D.; Zhu, Y.; Liu, L.; Ying, X.; Hsiung, C. E.; Sougrat, R.; Li, K.; Han, Y. Atomic-resolution transmission electron microscopy of electron beam—sensitive crystalline materials. *Science* **2018**, *359*, 675—679.

- (22) Aulakh, D.; Liu, L.; Varghese, J. R.; Xie, H.; Islamoglu, T.; Duell, K.; Kung, C. W.; Hsiung, C. E.; Zhang, Y.; Drout, R. J.; Farha, O. K.; Dunbar, K. R.; Han, Y.; Wriedt, M. Direct Imaging of Isolated Single-Molecule Magnets in Metal-Organic Frameworks. *J. Am. Chem. Soc.* 2019, 141, 2997–3005.
- (23) Li, Y.; Wang, K.; Zhou, W.; Li, Y.; Vila, R.; Huang, W.; Wang, H.; Chen, G.; Wu, G. H.; Tsao, Y.; Wang, H.; Sinclair, R.; Chiu, W.; Cui, Y. Cryo-EM Structures of Atomic Surfaces and Host-Guest Chemistry in Metal-Organic Frameworks. *Matter* **2019**, *1*, 428–438.
- (24) Shen, B.; Chen, X.; Shen, K.; Xiong, H.; Wei, F. Imaging the node-linker coordination in the bulk and local structures of metalorganic frameworks. *Nature Communications* 2020 11:1 2020, 11, 1–
- (25) Hovden, R.; Muller, D. A. Efficient elastic imaging of single atoms on ultrathin supports in a scanning transmission electron microscope. *Ultramicroscopy* **2012**, *123*, 59–65.
- (26) Egerton, R. F. Radiation damage to organic and inorganic specimens in the TEM. *Micron* **2019**, *119*, 72–87.
- (27) Reimer, L.; Khol, H. Transmission Electron Microscopy: Physics of Image Formation; Springer US: 2008.
- (28) Koshino, M.; Tanaka, T.; Solin, N.; Suenaga, K.; Isobe, H.; Nakamura, E. Imaging of Single Organic Molecules in Motion. *Science* **2007**, *316*, 853–853.
- (29) Koshino, M.; Niimi, Y.; Nakamura, E.; Kataura, H.; Okazaki, T.; Suenaga, K.; Iijima, S. Analysis of the reactivity and selectivity of fullerene dimerization reactions at the atomic level. *Nat. Chem.* **2010**, *2*, 117–124.
- (30) Mirzayev, R.; Mustonen, K.; Monazam, M. R. A.; Mittelberger, A.; Pennycook, T. J.; Mangler, C.; Susi, T.; Kotakoski, J.; Meyer, J. C. Buckyball sandwiches. *Science Advances* **2017**, *3*, No. e1700176.
- (31) Chamberlain, T. W.; et al. Stop-Frame Filming and Discovery of Reactions at the Single-Molecule Level by Transmission Electron Microscopy. *ACS Nano* **2017**, *11*, 2509–2520.
- (32) Mittelberger, A.; Kramberger, C.; Meyer, J. C. Insights into radiation damage from atomic resolution scanning transmission electron microscopy imaging of mono-layer CuPcCl16 films on graphene. *Sci. Rep.* **2018**, *8*, 6–12.
- (33) Vilas, J. L.; Tabassum, N.; Mota, J.; Maluenda, D.; Jiménez-Moreno, A.; Majtner, T.; Carazo, J. M.; Acton, S. T.; Sorzano, C. O. Advances in image processing for single-particle analysis by electron cryomicroscopy and challenges ahead. *Curr. Opin. Struct. Biol.* **2018**, 52, 127–145.
- (34) Cheng, Y. Single-particle cryo-EM-How did it get here and where will it go. *Science* **2018**, *361*, 876–880.
- (35) Lee, C.-H.; Khan, A.; Luo, D.; Santos, T. P.; Shi, C.; Janicek, B. E.; Kang, S.; Zhu, W.; Sobh, N. A.; Schleife, A.; Clark, B. K.; Huang, P. Y. Deep Learning Enabled Strain Mapping of Single-Atom Defects in Two-Dimensional Transition Metal Dichalcogenides with Sub-Picometer Precision. *Nano Lett.* **2020**, *20*, 3369–3377.
- (36) Scherer, S.; Kowal, J.; Chami, M.; Dandey, V.; Arheit, M.; Ringler, P.; Stahlberg, H. 2dx automator: Implementation of a semiautomatic high-throughput high-resolution cryo-electron crystallography pipeline. *J. Struct. Biol.* **2014**, *186*, 302–307.
- (37) Righetto, R. D.; Biyani, N.; Kowal, J.; Chami, M.; Stahlberg, H. Retrieving high-resolution information from disordered 2D crystals by single-particle cryo-EM. *Nat. Commun.* **2019**, *10*, 1722.
- (38) Yip, K. M.; Fischer, N.; Paknia, E.; Chari, A.; Stark, H. Atomicresolution protein structure determination by cryo-EM. *Nature* **2020**, 587, 157–161.
- (39) Nakane, T.; et al. Single-particle cryo-EM at atomic resolution. *Nature* **2020**, 587, 152–156.
- (40) Imran, M.; Ramzan, M.; Qureshi, A. K.; Khan, M. A.; Tariq, M. Emerging Applications of Porphyrins and Metalloporphyrins in Biomedicine and Diagnostic Magnetic Resonance Imaging. *Biosensors* 2018, 8, 95
- (41) de la Torre, G.; Claessens, C. G.; Torres, T. Phthalocyanines: old dyes, new materials. Putting color in nanotechnology. *Chem. Commun.* **2007**, 2000–2015.

- (42) Hendry, G. A.; Jones, O. T. Haems and chlorophylls: comparison of function and formation. *Journal of medical genetics* **1980**, *17*, 1–14.
- (43) Wang, T.; Kafle, T. R.; Kattel, B.; Liu, Q.; Wu, J.; Chan, W.-L. Growing Ultra-flat Organic Films on Graphene with a Face-on Stacking via Moderate Molecule-Substrate Interaction. *Sci. Rep.* **2016**, *6*. 28895.
- (44) Janicek, B. E.; Hinman, J. G.; Hinman, J. J.; hyun Bae, S.; Wu, M.; Turner, J.; Chang, H.-H.; Park, E.; Lawless, R.; Suslick, K. S.; Murphy, C. J.; Huang, P. Y. Quantitative Imaging of Organic Ligand Density on Anisotropic Inorganic Nanocrystals. *Nano Lett.* **2019**, *19*, 6308–6314.
- (45) Krivanek, O. L.; Chisholm, M. F.; Nicolosi, V.; Pennycook, T. J.; Corbin, G. J.; Dellby, N.; Murfitt, M. F.; Own, C. S.; Szilagyi, Z. S.; Oxley, M. P.; Pantelides, S. T.; Pennycook, S. J. Atom-by-atom structural and chemical analysis by annular dark-field electron microscopy. *Nature* **2010**, *464*, 571–574.
- (46) Wu, M.; Lander, G. C.; Herzik, M. A. Sub-2 Angstrom resolution structure determination using single-particle cryo-EM at 200 keV. *Journal of Structural Biology: X* **2020**, *4*, 100020.
- (47) Lee, Z.; Jeon, K.-J.; Dato, A.; Erni, R.; Richardson, T. J.; Frenklach, M.; Radmilovic, V. Direct Imaging of SoftHard Interfaces Enabled by Graphene. *Nano Lett.* **2009**, *9*, 3365–3369.
- (48) Pantelic, R. S.; Meyer, J. C.; Kaiser, U.; Stahlberg, H. The application of graphene as a sample support in transmission electron microscopy. *Solid State Commun.* **2012**, *152*, 1375–1382.
- (49) Huang, P. Y.; Kurasch, S.; Srivastava, A.; Skakalova, V.; Kotakoski, J.; Krasheninnikov, A. V.; Hovden, R.; Mao, Q.; Meyer, J. C.; Smet, J.; Muller, D. A.; Kaiser, U. Direct Imaging of a Two-Dimensional Silica Glass on Graphene. *Nano Lett.* **2012**, *12*, 1081–1086
- (50) Lee, J. K.; Bulut, I.; Rickhaus, M.; Sheng, Y.; Li, X.; Han, G. G.; Briggs, G. A. D.; Anderson, H. L.; Warner, J. H. Metal atom markers for imaging epitaxial molecular self-assembly on graphene by scanning transmission electron microscopy. *ACS Nano* **2019**, *13*, 7252–7260.
- (51) Han, Y.; Fan, X.; Wang, H.; Zhao, F.; Tully, C. G.; Kong, J.; Yao, N.; Yan, N. High-yield monolayer graphene grids for near-atomic resolution cryoelectron microscopy. *Proc. Natl. Acad. Sci. U. S. A.* **2020**, *117*, 1009–1014.
- (52) Algara-Siller, G.; Kurasch, S.; Sedighi, M.; Lehtinen, O.; Kaiser, U. The pristine atomic structure of MoS2 monolayer protected from electron radiation damage by graphene. *Appl. Phys. Lett.* **2013**, *103*, 203107.
- (53) Zan, R.; Ramasse, Q. M.; Jalil, R.; Georgiou, T.; Bangert, U.; Novoselov, K. S. Control of radiation damage in MoS2 by graphene encapsulation. *ACS Nano* **2013**, *7*, 10167–10174.
- (54) Jiang, X.; Xuan, S.; Kundu, J.; Prendergast, D.; Zuckermann, R. N.; Balsara, N. P. Effect of processing and end groups on the crystal structure of polypeptoids studied by cryogenic electron microscopy at atomic length scales. *Soft Matter* **2019**, *15*, 4723–4736.
- (55) Savitzky, B. H.; et al. Image registration of low signal-to-noise cryo-STEM data. *Ultramicroscopy* **2018**, *191*, 56–65.
- (56) Glaeser, R. M., Ed. Electron crystallography of biological macromolecules; Oxford University Press: 2007.
- (57) Pradère, P.; Revol, J. F.; Nguyen, L.; St. John Manley, R. Lattice imaging of poly-4-methyl-pentene-1 single crystals; use and misuse of fourier averaging techniques. *Ultramicroscopy* **1988**, 25, 69–80.
- (58) Kirkland, E. J. Computem: https://sourceforge.net/projects/computem/ (accessed May 26, 2020).
- (59) Saxton, W. O.; Baumeister, W. The correlation averaging of a regularly arranged bacterial cell envelope protein. *J. Microsc.* **1982**, 127, 127–138.
- (60) Tang, G.; Peng, L.; Baldwin, P. R.; Mann, D. S.; Jiang, W.; Rees, I.; Ludtke, S. J. EMAN2: An extensible image processing suite for electron microscopy. *J. Struct. Biol.* **2007**, *157*, 38–46.
- (61) Bell, J. M.; Chen, M.; Baldwin, P. R.; Ludtke, S. J. High resolution single particle refinement in EMAN2.1. *Methods* **2016**, *100*, 25–34.

(62) Brown, C. J. Crystal structure of β-copper phthalocyanine. Journal of the Chemical Society A: Inorganic, Physical, Theoretical 1968, 0, 2488–2493.